Uranium and Lanthanide Complexes with the 2-Mercapto Benzothiazolate Ligand: Evidence for a Specific Covalent Binding Site in the Differentiation of Isostructural Lanthanide(III) and Actinide(III) Compounds

Mathieu Roger,[†] Lotfi Belkhiri,[‡] Thérèse Arliguie,*[,†] Pierre Thuéry,[†] Abdou Boucekkine,*[,§] and Michel Ephritikhine*[,†]

Service de Chimie Moléculaire, DSM, DRECAM, CNRS URA 331, CEA/Saclay 91191 Gif-sur-Yvette, France, Laboratoire de Chimie Moléculaire (LACMOM), Département de Chimie, Faculté des Sciences, Université Mentouri de Constantine, BP 325, Route de l'Aéroport Ain El Bey, 25017 Constantine, Algeria, and UMR CNRS 6226 Sciences Chimiques de Rennes, Université de Rennes 1, Campus de Beaulieu, 35042 Rennes, France

Received July 20, 2007

Treatment of $[U(Cp^*)_2Cl_2]$ with KSBT in THF gave $[U(Cp^*)_2(SBT)_2]$, which exhibits the usual bent sandwich configuration in the solid state with the two SBT ligands adopting the bidentate ligation mode. The monocyclopentadienyl compound $[U(Cp^*)(SBT)_3]$ was synthesized by reaction of $[U(Cp^*)(BH_4)_3]$ with KSBT in THF, and its reduction with potassium amalgam in the presence of 18-crown-6 afforded the corresponding anionic complex $[K(18\text{-crown-}6)(THF)_2][U(Cp^*)(SBT)_3]$. The lanthanide analogues $[K(THF)_2Ln(Cp^*)(SBT)_3]$ were obtained by treating $[Ln(BH_4)_3(THF)_3]$ with KSBT and KCp*; isomorphous crystals of $[K(15\text{-crown-}5)_2][Ln(Cp^*)(SBT)_3]\cdot THF$ [Ln = La, Ce, Nd] were formed upon addition of 15-crown-5. Comparison of the crystal structures of the pentagonal bipyramidal complexes $[M(Cp^*)(SBT)_3]^-$ reveals that the $M-N_{ax}$ distances are shorter than the $M-N_{eq}$ distances, whatever the metal, the phenomenon being enhanced in the U(III) compound versus the Ln(III) analogues. The structural data obtained by relativistic density functional theory (DFT) calculations reproduce experimental trends. Electronic population and molecular orbital analyses show that the structural differences in the series of $[M(Cp^*)(SBT)_3]^-$ anions are related to the uranium 5f orbital−ligand mixing, which is greater than the lanthanide 4f orbital−ligand mixing. Moreover, the consideration of the corresponding bond orders and the analysis of the bonding energy bring to light a strong and specific interaction between the uranium and apical nitrogen atoms.

Introduction

As a heterocyclic thionate ligand with potential S and N donors, the 2-mercapto benzothiazolate ligand (SBT) endows a variety of main group and d transition-metal complexes with interesting structural and reactivity features.[1] Special attention was paid to the SBT complexes for their biological activities[2] and their applications as anticorrosion agents and accelerators in the rubber vulcanization processes.[3] The SBT ligand in mononuclear complexes can adopt either a monodentate coordination mode, bonding to metal ions through N or exocyclic S atoms, or a bidentate chelating mode, as shown in Scheme 1. Polynuclear complexes were also obtained, in which the SBT group acts as a bridging ligand between two,[4a] three,[4b] and even four metal centers;[4c] the presence of N and S atoms of distinct softness favors the building of hetero- or homopolynuclear complexes with the metals in different oxidation states. However, the SBT ligand has been almost ignored in f-element chemistry, the compounds so far reported being limited to the lanthanide complexes $[Ln(C_5H_4R)_2(SBT)(THF)]$ (R = H and Ln = Y, Sm, Dy, Yb,[5a] and Tm;[5b] R = $SiMe_2{}^tBu$ and Ln = Er[6]) and $[Ln(SBT)Cl_2][Ln(OH)_3]\cdot xH_2O$,[7] and to the homoleptic

Scheme 1. Two Hybrid Forms of the Chelating SBT Ligand

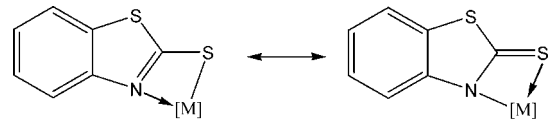

I II

* To whom correspondence should be addressed. E-mail: (T.A.) therese.arliguie@cea.fr, (A.B.) abdou.boucekkine@univ-rennes1.fr, (M.E.) michel.ephritikhine@cea.fr.

† CEA/Saclay.

‡ Université de Constantine.

§ CNRS-Université de Rennes.

(1) (a) Raper, E. S. *Coord. Chem. Rev.* **1996**, *153*, 199. (b) Raper, E. S. *Coord. Chem. Rev.* **1997**, *165*, 475.

(2) (a) Marchesi, E.; Marchi, A.; Marvelli, L.; Peruzzini, M.; Brugnati, M.; Bertolasi, V. *Inorg. Chim. Acta* **2005**, *358*, 352. (b) Brugnati, M.; Marchesi, E.; Marchi, A.; Marvelli, L.; Bertolasi, V.; Ferretti, V. *Inorg. Chim. Acta* **2005**, *358*, 363.

(3) McCleverty, J. A.; Morrison, N. J.; Spencer, N.; Ashworth, C. C.; Bailey, N. A.; Johnson, M. R.; Smith, J. M. A.; Tabbiner, B. A.; Taylor, C. R. *J. Chem. Soc., Dalton Trans.* **1980**, 1945.

(4) (a) Ciriano, M. A.; Pérez-Torrente, J. J.; Lahoz, F. J.; Oro, L. A. *Inorg. Chem.* **1992**, *31*, 969. (b) Ciriano, M. A.; Pérez-Torrente, J. J.; Oro, L. A.; Tiripicchio, A.; Tiripicchio-Camellini, M. *J. Chem. Soc., Dalton Trans.* **1991**, 255. (c) Ciriano, M. A.; Sebastián, S.; Oro, L. A.; Tiripicchio, A.; Tiripicchio-Camellini, M.; Lahoz, F. J. *Angew. Chem., Int. Ed. Engl.* **1988**, *27*, 402.

(5) (a) Zhang, L. X.; Zhou, X. G.; Huang, Z. E.; Cai, R. F.; Huang, X. Y. *Polyhedron* **1999**, *18*, 1533. (b) Zhang, L. X.; Zhou, X. G.; Huang, Z. E.; Cai, R. F.; Zhang, L. B.; Wu, Q. J. *Chin. J. Str. Chem.* **2001**, *20*, 40.

(6) Zhou, X. G.; Zhang, L. X.; Zhang, C. M.; Zhang, J.; Zhu, M.; Cai, R. F.; Huang, Z. E.; Huang, Z. X.; Wu, Q. J. *J. Organomet. Chem.* **2002**, *655*, 120.

(7) Zhang, Q. J.; Wei, F. X.; Zhang, W. G.; Huang, M. Y.; Luo, Y. F. *J. Rare Earths* **2002**, *20*, 395.

10.1021/om7007315 CCC: $40.75
Publication on Web 12/20/2007

thorium complex $[Th(SBT)_4]$;[8] only the organometallic derivatives were properly characterized with the X-ray crystal structures of $[Ln(C_5H_5)_2(SBT)(THF)]$ (Ln = Tm, Yb, Dy) and $[Er(C_5H_4SiMe_2{}^tBu)_2(SBT)(THF)]$. We were interested in developing this class of compounds, especially with complexes of the uranium(III) ion which, being less hard than the lanthanide(III) and uranium(IV) ions, could possibly present distinct characteristics of the SBT ligation. Heterocyclic thionate ligands are indeed attractive for the study of lanthanide(III)/actinide(III) differentiation, which represents an important problem for both its fundamental aspects, i.e., the precise knowledge of the metal–ligand bonding and the respective role of the 4f and 5f electrons, and its applications, particularly in the management of nuclear wastes.[9] Here, we present the synthesis and structural characterization of the organouranium(IV) derivatives $[U(Cp^*)_2(SBT)_2]$ and $[U(Cp^*)(SBT)_3]$ ($Cp^* = \eta$-C_5Me_5) and the series of trivalent complexes $[M(Cp^*)(SBT)_3]^-$ (M = U, La, Ce, Nd).

Comparison of the crystal structures of a variety of isostructural trivalent lanthanide (Ln) and uranium complexes showed that, taking into account the variation in the ionic radii of the metals, the bonds between the 5f-element and the soft and/or π-accepting ligands are shorter than the corresponding bonds in the lanthanide counterpart. This shortening is explained by a modest enhancement of covalence in the actinide versus lanthanide−ligand bonding.[10] This difference plays an essential role in the selective complexation of trivalent 5f over 4f ions.[9] However, for all the pairs of analogous Ln(III) and U(III) complexes which have been crystallographically characterized, there is no indication that specific bonds play a distinct role in the differentiation. The occurrence of such a situation is, however, plausible since distinctively long and short M−X bonds were simultaneously found in a same compound, a typical example being provided by the octahedral actinide (An) complexes $[AnOX_5]^{n-}$ (X = F, Cl, Br; n = 0, 1, 2 for An = Np, U, Pa, respectively) in which the *trans* An−X distances are shorter than the *cis* An−X distances due to the occurrence of the *inverse trans* influence phenomenon.[11] The series of $[M(Cp^*)(SBT)_3]^-$ anions (M = U, La, Ce, Nd) provides a first evidence of the presence of a specific covalent binding site in discrimination between Ln(III) and An(III) complexes; in these pentagonal bipyramidal complexes, the peculiar behavior of the axial M−N bond was revealed by the X-ray crystal structures and analyzed by relativistic density functional theory (DFT).

Results and Discussion

Synthesis of the Complexes. Treatment of $[U(Cp^*)_2Cl_2]$[12] with 1 and 2 molar equiv of KSBT in THF readily afforded $[U(Cp^*)_2(SBT)Cl]$ (**1**) and $[U(Cp^*)_2(SBT)_2]$ (**2**), which were extracted in toluene and isolated as brown powders in 91 and 95% yield, respectively (eqs 1 and 2). Crystals of $[U(Cp^*)_2(SBT)_2]\cdot THF$ (**2**·THF) suitable for X-ray diffraction analysis (vide infra) were obtained by crystallization from THF. The ^1H NMR spectra of **1** and **2** exhibit four signals of equal intensities, two doublets and two triplets, attributed to the SBT ligands, which are equivalent in **2**, and a singlet corresponding to the equivalent Cp* ligands.

$$[U(Cp^*)_2Cl_2] + KSBT \xrightarrow{THF} \underset{(\mathbf{1})}{[U(Cp^*)_2(SBT)Cl]} + KCl \quad (1)$$

$$[U(Cp^*)_2Cl_2] + 2KSBT \xrightarrow{THF} \underset{(\mathbf{2})}{[U(Cp^*)_2(SBT)_2]} + 2KCl \quad (2)$$

Reduction of **2** with sodium or potassium amalgam in THF, in the presence or absence of 18-crown-6 ether, did not give the corresponding U(III) anionic complex $[U(Cp^*)_2(SBT)_2]^-$. The ^1H NMR spectrum of the reaction mixture revealed the formation of a new compound, which was subsequently identified as the $[U(Cp^*)(SBT)_3]^-$ anion and obviously resulted from ligand redistribution reaction of the unstable $[U(Cp^*)_2(SBT)_2]^-$ species.

The monocyclopentadienyl compound $[U(Cp^*)(SBT)_3]$ (**3**) was synthesized by reaction of $[U(Cp^*)(BH_4)_3]$[13] with 3 molar equiv of KSBT in THF (eq 3); after filtration and evaporation, the product was isolated as a red powder in 83% yield, and red crystals were obtained by crystallization from THF.

$$[U(Cp^*)(BH_4)_3] + 3KSBT \xrightarrow{THF} \underset{(\mathbf{3})}{[U(Cp^*)(SBT)_3]} + 3KBH_4 \quad (3)$$

The sodium or potassium amalgam reduction of **3** in THF in the presence of 18-crown-6 led to the formation of $[U(Cp^*)(SBT)_3]^-$ (eq 4); the presence of the crown ether is necessary to avoid rapid decomposition of the anion into unidentified products. After usual workup, the brown powder

(8) (a) Spacu, G.; Pirtea, T. I. *Acad. Rep. Populare Romane, Bul. Stiint., Ser.: Mat., Fiz., Chim.* **1950**, *2*, 669. (b) Johri, K. N.; Kaushik, N. K.; Venugopalan, K. A. *J. Therm. Anal.* **1976**, *10*, 47.

(9) (a) Nash, K. L. *Solvent Extr. Ion Exch.* **1993**, *11*, 729. (b) Nash, K. L. Separation chemistry for lanthanides and trivalent actinides. In *Handbook on the physics and chemistry of rare earths*; Gschneidner K. A., Jr., Eyring, L., Choppin, G. R., Lander, G. H., Eds.; Elsevier Science: New York, 1994; Vol. 18 (121), p 197. (c) Actinides and Fission Products Partitioning and Transmutation. Status and Assessment Report; NEA/OECD Report; NEA/OECD: Paris, 1999. (d) Implications of Partitioning and Transmutation in Radioactive Waste Management.; IAEA - TRS 435; IAEA, Vienna, Austria, 2005.

(10) (a) Brennan, J. G.; Stults, S. D.; Andersen, R. A.; Zalkin, A. *Organometallics* **1988**, *7*, 1329. (b) Wietzke, R.; Mazzanti, M.; Latour, J. M.; Pécaut, *J. Inorg. Chem.* **1999**, *38*, 3581. (c) Wietzke, R.; Mazzanti, M.; Latour, J. M.; Pécaut, J. *J. Chem. Soc., Dalton Trans.* **2000**, 4167. (d) Iveson, P. B.; Rivière, C.; Guillaneux, D.; Nierlich, M.; Thuéry, P.; Ephritikhine, M.; Madic, C. *Chem. Commun.* **2001**, 1512. (e) Rivière, C.; Nierlich, M.; Ephritikhine, M.; Madic, C. *Inorg. Chem.* **2001**, *40*, 4428. (f) Berthet, J. C.; Rivière, C.; Miquel, Y.; Nierlich, M.; Madic, C.; Ephritikhine, M. *Eur. J. Inorg. Chem.* **2002**, 1439. (g) Berthet, J. C.; Miquel, Y.; Iveson, P. B.; Nierlich, M.; Thuéry, P.; Madic, C.; Ephritikhine, M. *J. Chem. Soc., Dalton Trans.* **2002**, 3265. (h) Mazzanti, M.; Wietzke, R.; Pécaut, J.; Latour, J. M.; Maldivi, P.; Remy, M. *Inorg. Chem.* **2002**, *41*, 2389. (i) Karmazin, L.; Mazzanti, M.; Pécaut, J. *Chem. Commun.* **2002**, 654. (j) Cendrowski-Guillaume, S. M.; Le Gland, G.; Nierlich, M.; Ephritikhine, M. *Eur. J. Inorg. Chem.* **2003**, 1388. (k) Berthet, J. C.; Nierlich, M.; Ephritikhine, M. *Polyhedron* **2003**, *22*, 3475. (l) Karmazin, L.; Mazzanti, M.; Bezombes, J. P.; Gateau, C.; Pécaut, J. *Inorg. Chem.* **2004**, *43*, 5147. (m) Guillaumont, D. *J. Phys. Chem. A* **2004**, *108*, 6893. (n) Mehdoui, T.; Berthet, J. C.; Thuéry, P.; Ephritikhine, M. *Dalton Trans.* **2004**, 579. (o) Mehdoui, T.; Berthet, J. C.; Thuéry, P.; Ephritikhine, M. *Eur. J. Inorg. Chem.* **2004**, 1996. (p) Mehdoui, T.; Berthet, J. C.; Thuéry, P.; Ephritikhine, M. *Dalton Trans.* **2005**, 1263. (q) Berthet, J. C.; Nierlich, M.; Miquel, Y.; Madic, C.; Ephritikhine, M. *Dalton Trans.* **2005**, 369. (r) Mehdoui, T.; Berthet, J. C.; Thuéry, P.; Salmon, L.; Rivière, E.; Ephritikhine, M. *Chem. Eur. J.* **2005**, *11*, 6994. (s) Roger, M.; Belkhiri, L.; Thuéry, P.; Arliguie, T.; Fourmigué, M.; Boucekkine, A.; Ephritikhine, M. *Organometallics* **2005**, *24*, 4940. (t) Roger, M.; Barros, N.; Arliguie, T.; Thuéry, P.; Maron, L.; Ephritikhine, M. *J. Am. Chem. Soc.* **2006**, *128*, 8790.

(11) (a) O'Grady, E.; Kaltsoyannis, N. *J. Chem. Soc., Dalton Trans.* **2002**, 1233. (b) Chermette, H.; Rachedi, K.; Volatron, F. *THEOCHEM* **2006**, *762*, 109.

(12) Fagan, P. J.; Manriquez, J. M.; Maatta, E. A.; Seyam, A. M.; Marks, T. J. *J. Am. Chem. Soc.* **1981**, *103*, 6650.

(13) Gradoz, P.; Baudry, D.; Ephritikhine, M.; Lance, M.; Nierlich, M.; Vigner, J. *J. Organomet. Chem.* **1994**, *466*, 107.

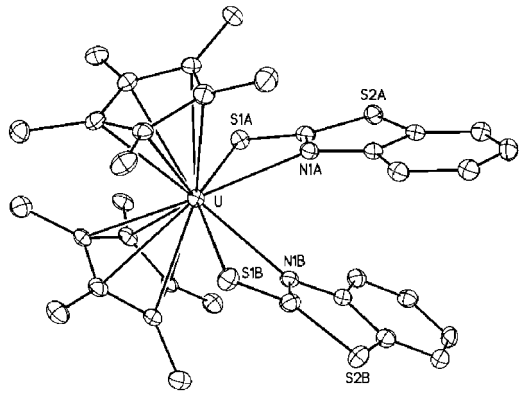

Figure 1. View of complex **2**. Hydrogen atoms have been omitted. Displacement parameters are drawn at the 30% probability level.

of [Na(18-crown-6)(THF)][U(Cp*)(SBT)$_3$] was isolated in 79% yield; dark brown crystals of [K(18-crown-6)(THF)$_2$][U(Cp*)(SBT)$_3$] (**4**) were grown by slow diffusion of pentane into a THF solution. Compounds **1**−**4** are first examples of SBT complexes of uranium.

$$[U(Cp^*)(SBT)_3] + K(Hg) + 18\text{-crown-}6 \xrightarrow{THF}$$

$$[K(18\text{-crown-}6)(THF)_2][U(Cp^*)(SBT)_3] \quad (4)$$
$$(\mathbf{4})$$

Successive treatment of [Ln(BH$_4$)$_3$(THF)$_3$][14] with 3 molar equiv of KSBT and one mole equivalent of KCp* in THF gave, after filtration and evaporation, a colorless (La), yellow (Ce) or blue (Nd) powder of [K(THF)$_2$Ln(Cp*)(SBT)$_3$] in 71, 90 and 60% yield, respectively (eq 5); isomorphous crystals of [K(15-crown-5)$_2$][Ln(Cp*)(SBT)$_3$]•THF [Ln = La (**5**), Ce (**6**), Nd (**7**)] were formed upon addition of 15-crown-5.

$$[Ln(BH_4)_3(THF)_3] + 3KSBT + KCp^* \xrightarrow{THF}$$

$$[K(THF)_2Ln(Cp^*)(SBT)_3] + 3KBH_4 \quad (5)$$

Structure of the Complexes in the Crystal and in Solution. A view of **2** is shown in Figure 1, while selected bond lengths and angles of all the complexes are listed in Table 1. The bis(Cp*) compound is found in the usual bent sandwich configuration, with the SBT ligands A and B adopting the bidentate ligation mode; the line joining the U atom and the middle of the N(1A)−N(1B) segment is a pseudo C_2 axis. The average U−C distance and the ring centroid−U−ring centroid angle of 2.796(15) Å and 123° can be compared with the values of 2.788(13) Å and 138° in [U(Cp*)$_2$(η^2-CONMe$_2$)$_2$][15] and 2.75(2) Å and 137° in [U(Cp*)$_2$(η^2-N$_2$C$_3$H$_3$)$_2$],[16] the two other compounds of the type [U(Cp*)$_2$(η^2-ligand)$_2$] to have been crystallographically characterized. The S(1) atoms lie in the equatorial girdle, while N(1A) and N(1B) are displaced on either side of this plane, by 1.084(4) and 1.148(4) Å, respectively; this deviation is likely due to the steric hindrance of the SBT ligands which are rotated out of the equatorial plane by 20.24(8) and 23.37(9)°. Such a situation was encountered in the bis(carbamoyl) complex [U(Cp*)$_2$(η^2-CONMe$_2$)$_2$][15] where the two planar CONMe$_2$ ligands form angles of 13.2 and 15.4° with the equatorial girdle, but not in the pyrazolate derivative [U(Cp*)$_2$(η^2-N$_2$C$_3$H$_3$)$_2$][16] where the two nitrogen ligands are coplanar. The average U−N distance of 2.5885(5) Å is larger than in the amide and pyrazolate compounds [U(Cp*)$_2$(NH{C$_6$H$_3$Me$_2$-2,6})$_2$] [2.267(6) Å][17] and [U(Cp*)$_2$(η^2-N$_2$C$_3$H$_3$)$_2$] [2.38(2) Å][16] and smaller than in the pyrazole adduct [U(Cp*)$_2$Cl$_2$(η^1-N$_2$C$_3$H$_3$)] [2.607(8) Å].[16] The average U−S distance of 2.862(7) Å is larger than in the thiolate complex [U(Cp*)$_2$(SMe)$_2$] [2.639(3) Å][18] and can be compared with that of 2.90(2) Å in the trithiocarbonate ligand of [U(C$_5$Me$_5$)$_2$(S^{t}Bu)(S$_2$CS^{t}Bu)].[18] The mean C(1)−S(1) and C(1)−N(1) bond lengths of 1.713(5) and 1.3225(5) Å in **2** are identical to those of 1.70(1) and 1.31(1) Å found in [Yb(C$_5$H$_5$)$_2$(SBT)(THF)][5a] and [Er(C$_5$H$_4$SiMe$_2$^{t}Bu)$_2$(SBT)-(THF)];[6] these values are intermediate between the corresponding C−S distances [1.662(4) and 1.771 Å] and C−N distances [1.353(6) and 1.262 Å] in benzothiazole-2-thione[19] and 2-methylthiobenzothiazole,[20] respectively, and reflect, as well as the U−S and U−N distances, the thionate character of the SBT ligand.

A view of **3** is shown in Figure 2. The configuration can be described as a distorted pentagonal bipyramid, if the Cp* ligand is considered to occupy a single site of coordination. The equatorial base which contains N(1A), N(1C), S(1A), S(1B), and S(1C), with an rms deviation of 0.18 Å, is parallel to the five-membered ring and orthogonal to the plane defined by the metal center, the ring centroid, and the atoms of the SBT ligand labeled B [rms deviation of 0.05 Å]; this plane is a pseudomirror plane for the complex. The U atom is at 0.6789(11) Å from the equatorial plane toward the cyclopentadienyl ligand, and the two planes defined, respectively, by the U, N(1A), S(1A) and U, N(1C), S(1C) atoms of the SBT ligands A and C form a dihedral angle of 154.9(2)°. The average U−S distance is similar to that in **2** while the mean U−N distance is 0.08 Å smaller; this difference would be explained by the lesser steric congestion of the mono(Cp*) compound. It is however interesting to note that the U−S and U−N bond lengths of the SBT ligand B are, respectively, 0.05 Å larger and 0.09 Å smaller than the U−S and U−N distances of the other two SBT ligands A and C; in connection with this trend, the C−S(1) and C−N(1) bond lengths of ligand B seem to be smaller and larger, respectively, than those in ligands A and C. These structural features could indicate that the contribution of the thioketone/metal amido canonical form (II in Scheme 1) to the true structure of the SBT ligand is more important in ligand B than in ligands A and C of **3**. Such shortening of the metal−axial ligand vs metal−equatorial ligand bond distances was found in the phosphoylide uranium complex [U(C$_5$H$_5$){(CH$_2$)(CH$_2$)PPh$_2$}$_3$] and was explained by extended Hückel molecular orbital calculations showing a larger overlap population for the axial U−C(ylide) bond, which thus exhibits a more covalent character.[21] Similar differences between axial and equatorial metal–ligand bonds have been observed in a variety of pentagonal bipyramidal transition-metal compounds.[22–24] In particular, in the zirconium complex [Zr(C$_5$H$_5$)(CF$_3$COCHCOCF$_3$)$_3$], which adopts the same coor-

(14) (a) Roger, M.; Arliguie, T.; Thuéry, P.; Fourmigué, M.; Ephritikhine, M. *Inorg. Chem.* **2005**, *44*, 584. (b) Mirsaidov, U.; Rotenberg, T. G.; Dymova, D. T. N. *Akad. Nauk. SSSR* **1976**, *19*, 30.
(15) Fagan, P. J.; Manriquez, J. M.; Vollmer, S. H.; Day, S. C.; Day, V. W.; Marks, T. J. *J. Am. Chem. Soc.* **1981**, *103*, 2206.
(16) Eigenbrot, C. W. J.; Raymond, K. N. *Inorg. Chem.* **1982**, *21*, 2653.
(17) Straub, T.; Frank, W.; Reiss, G. J.; Eisen, M. *J. Chem. Soc., Dalton Trans.* **1996**, 2451.
(18) Lescop, C.; Arliguie, T.; Lance, M.; Nierlich, M.; Ephritikhine, M. *J. Organomet. Chem.* **1999**, *580*, 137.
(19) Chesick, J. P.; Donohue, J. *Acta Crystallogr., Sect. B* **1971**, *27*, 1441.
(20) Wheatley, P. J. *J. Chem. Soc.* **1962**, 3636.
(21) Cramer, R. E.; Mori, A. L.; Maynard, R. B.; Gilje, J. W.; Tatsumi, K.; Nakamura, A. *J. Am. Chem. Soc.* **1984**, *106*, 5920.
(22) Fay, R. C. *Coord. Chem. Rev.* **1996**, *154*, 99.

Table 1. Selected Bond Lengths (Å) and Angles (deg) in Complexes 2–7

compound	ligand	M–S(1)	M–N(1)	C(1)–N(1)	C(1)–S(1)	N(1)–M–S(1)	<M–C>
$[U(Cp^*)_2(SBT)_2]$•THF							
	A	2.8684(12)	2.589(4)	1.322(6)	1.718(5)	57.89(9)	
	B	2.8546(12)	2.588(4)	1.323(6)	1.708(5)	58.01(9)	
	avg	2.862(7)	2.5885(5)	1.3225(5)	1.713(5)	57.95(6)	2.80(2)
$[U(Cp^*)(SBT)_3]$							
	A	2.8264(10)	2.541(3)	1.313(5)	1.723(4)	59.01(8)	
	B	2.8736(11)	2.448(4)	1.333(5)	1.706(4)	59.66(8)	
	C	2.8151(11)	2.541(3)	1.325(5)	1.715(4)	59.34(8)	
	avg	2.84(3)	2.51(4)	1.324(8)	1.715(7)	59.3(3)	2.72(2)
$K^*[U(Cp^*)(SBT)_3]$[a]							
	A	2.9081(16)	2.662(5)	1.320(8)	1.706(6)	57.24(11)	
	B	2.9704(17)	2.562(5)	1.324(8)	1.717(7)	57.20(12)	
	C	2.9758(15)	2.643(5)	1.317(8)	1.699(7)	56.29(11)	
	avg	2.95(3)	2.62(4)	1.320(3)	1.707(7)	56.9(4)	2.768(4)
$K^*[La(Cp^*)(SBT)_3]$•THF[b]							
	A	2.987(2)	2.659(7)	1.321(11)	1.710(8)	56.48(16)	
	B	3.025(2)	2.632(7)	1.312(11)	1.706(9)	56.00(15)	
	C	2.993(2)	2.658(7)	1.314(11)	1.715(9)	56.56(15)	
	avg	3.00(2)	2.650(12)	1.316(4)	1.710(4)	56.3(2)	2.82(2)
$K^*[Ce(Cp^*)(SBT)_3]$•THF[b]							
	A	2.966(3)	2.639(8)	1.313(13)	1.741(11)	57.2(2)	
	B	2.995(3)	2.610(9)	1.347(13)	1.683(11)	56.7(2)	
	C	2.976(3)	2.636(8)	1.322(12)	1.733(11)	57.25(19)	
	avg	2.979(12)	2.628(13)	1.327(14)	1.72(3)	57.1(2)	2.78(2)
$K^*[Nd(Cp^*)(SBT)_3]$•THF[b]							
	A	2.926(3)	2.614(7)	1.273(12)	1.749(10)	57.29(19)	
	B	2.961(3)	2.578(7)	1.314(12)	1.691(10)	57.16(18)	
	C	2.941(2)	2.611(8)	1.314(12)	1.707(10)	57.22(19)	
	avg	2.943(14)	2.60(2)	1.30(2)	1.72(2)	57.22(5)	2.777(3)

[a] K^* = K(18-crown-6)$(THF)_2$. [b] K^* = $K(15\text{-crown-5})_2$.

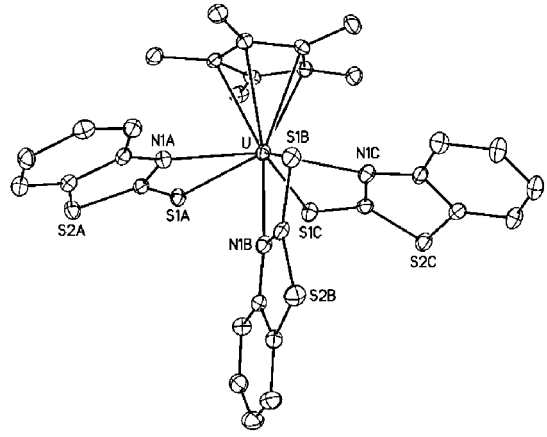

Figure 2. View of complex **3**. Hydrogen atoms have been omitted. Displacement parameters are drawn at the 30% probability level.

dination geometry as $[U(Cp^*)(SBT)_3]$, the Zr−O distances of the two equatorial acetylacetonate ligands average 2.225(11) Å, while those of the unique bidentate ligand are 2.166(6) and 2.266(6) Å for the axial and equatorial positions, respectively.[23] Ab initio calculations indicated that the site preference in transition-metal seven-coordinate complexes would result from the anisotropy in electron distribution associated with the metal nonbonding d orbitals.[24]

The pentagonal bipyramidal solid state structure of **3** is retained in solution, as shown by the ^{1}H NMR spectra which exhibit two sets of four signals in the intensity ratio of 2:1, corresponding to the two equatorial SBT ligands A and C and the unique SBT ligand B, respectively; coalescence of these signals was observed at ca. 100 °C, and the high-limit spectrum was not obtained.

The $[M(Cp^*)(SBT)_3]^-$ anions of the trivalent uranium and lanthanide compounds **4**−**7** adopt the same pentagonal bipyramidal configuration as the neutral uranium(IV) complex **3**. The U−S and U−N distances in **4** which average 2.95(3) and 2.62(4) Å (Table 1) are 0.11 Å larger than in **3**, while a difference of 0.15 Å is expected from the variation in the radii of the U^{4+} and U^{3+} ions;[25] the average bite angle of the SBT ligands is smaller, by ca. 2.4°. As observed with the uranium complexes **3** and **4** and the lanthanide compounds $[Ln(C_5H_4R)_2(SBT)(THF)]$ (R = H and Ln = Dy, Yb[5a] and Tm;[5b] R = $SiMe_2{}^tBu$ and Ln = Er[6]), the Ln−N and Ln−S distances in **5**–**7** are intermediate between typical σ and donating bond lengths, and the average C(1)−N(1) and C(1)−S(1) bond lengths are intermediate between single and double bond lengths, reflecting the thionate character of the SBT ligand.

The ^{1}H NMR spectra of the $[M(Cp^*)(SBT)_3]^-$ anions indicate that the pentagonal bipyramidal structure found in the crystal is also that adopted in solution. These trivalent complexes are more fluxional than the uranium(IV) counterpart, the coalescence of the SBT signals being observed at lower temperatures comprised between ca. 30 °C (Nd) and −10 °C (La). This difference can be explained by the larger ionic radii of the metals in the trivalent ionic compounds, which would facilitate the intramolecular exchange of the SBT ligands. Unfortunately, the coalescence temperatures cannot be measured with a high precision and the line-shape analysis of the spectra cannot be performed with a good accuracy, so that lanthanide(III)/actinide(III) differentiation cannot be evidenced with confidence from the NMR spectra of the $[M(Cp^*)(SBT)_3]^-$ anions.

Comparison of the Crystal Structures of the Analogous Uranium(III) and Lanthanide(III) Complexes. In contrast to the structure of $[K(18\text{-crown-6})(THF)_2][U(Cp^*)(SBT)_3]$ (**4**),

(23) Elder, M. *Inorg. Chem.* **1969**, *8*, 2103.

(24) (a) Hoffmann, R.; Beier, B. F.; Muetterties, E. L.; Rossi, A. R. *Inorg. Chem.* **1977**, *16*, 511. (b) Maseras, F.; Li, X. K.; Koga, N.; Morokuma, K. *J. Am. Chem. Soc.* **1993**, *115*, 10974.

(25) Shannon, R. D. *Acta Crystallogr., Sect. A.* **1976**, *32*, 751.

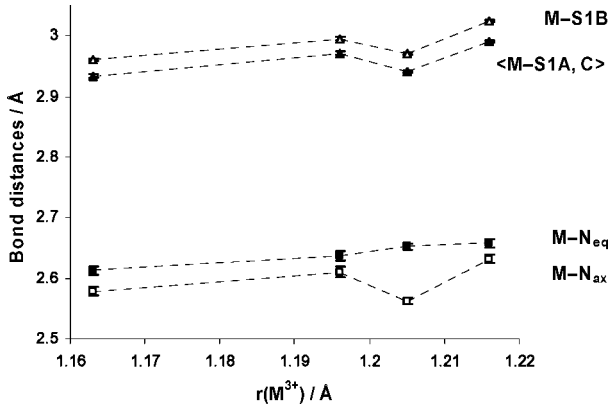

Figure 3. M−N (squares) and M−S (triangles) bond lengths for the SBT ligands A and C (closed symbols) and the unique SBT ligand B (open symbols) in the $[M(Cp^*)(SBT)_3]^-$ complexes as a function of the metal ionic radii. Lines are guides for the eye.

which was refined to a R_1 factor of 0.045, intractable disorder of the two 15-crown-5 and THF molecules in the structures of $[K(15\text{-crown-}5)_2][Ln(Cp^*)(SBT)_3]\bullet THF$ (**5**–**7**) led to R_1 factors of ca. 0.10. However, this disorder does not affect the anionic lanthanide complex, in particular the metal–ligand bond distances and angles, which can be confidently considered as properly characterized. The configurations of the anions of **4** and **5**–**7** exhibit only small differences. The pentagonal bipyramidal coordination geometry is slightly more distorted in the lanthanide complexes, as shown by the rms deviations of the S(1) and N(1) atoms of the SBT ligands A and C from their mean plane and the distance of S(1B) from this plane, 0.046–0.053 and 0.836(12)–0.933(10) Å, respectively, instead of 0.008 and 0.609(8) Å in the uranium(III) counterpart; the rms deviations of the five equatorial donor atoms from their mean plane are in the range 0.21–0.23 Å in the lanthanide complexes and 0.15 Å in the U(III) complex, the metal atom being respectively at 0.692(3)–0.706(2) (Ln) and 0.743(2) Å (U) from this plane; the dihedral angle between the M−N(1A)−S(1A) and M−N(1C)−S(1C) planes is 22.3(3)–23.1(3)° and 27.2(2)° for M = Ln and U, respectively.

The plots of the M−X(1B) distances and the average M−X(1A) and M−X(1C) distances (X = S and N) as a function of the ionic radii $r(M^{3+})$ of the metals in the anionic compounds **4**–**7** are shown in Figure 3. In all of the complexes, and as observed in the uranium(IV) compound **3**, the axial M−N(1B) bond ($M-N_{ax}$) is shorter than the equatorial M−N(1A) and M−N(1C) bonds ($M-N_{eq}$); in connection with this trend, the M−S distance of the SBT ligand B is slightly longer than those of ligands A and C (Table 1). For the lanthanide complexes **5**–**7**, a linear relationship is observed between the Ln−S or Ln−N distances and $r(Ln^{3+})$, with the r^2 coefficients of the regression lines larger than 0.98; this trend reflects the essentially ionic character of the bonds. The dots corresponding to the U−S and $U-N_{ax}$ distances of the uranium(III) complex **4** are displaced from the linear plots of the Ln−S and $Ln-N_{ax}$ distances and correspond to values lower than those expected from a purely ionic bonding model. The shortening of the U−S and $U-N_{ax}$ distances by 0.04 and 0.06 Å, respectively, seems significant since it is larger than the difference due to the variation of the ionic radii of the lanthanide ions, which is nicely reflected in the variation of the Ln−S and Ln−N distances. Such deviations Δ corresponding to the differences [<U−X> − <Ln−X>] and $[r(U^{3+}) - r(Ln^{3+})]$ were detected in a variety of analogous uranium(III) and lanthanide(III) complexes and were explained by a greater covalent contribution to the U−X bond (X = C, N, P, S, I).[10] These deviations are generally equal to 0.02–0.05 Å, but are as high as 0.1 Å in the phosphorus complexes $[M(C_5H_4Me)_3(L)]$ [M = Ce or U; L = PMe_3 or $P(OCH_2)_3CEt$][10a] and in the bipyridine compounds $[M(Cp^*)_2(bipy)]I$ (M = U, Ce),[10q] and Δ = 0.2 Å in the terpyridine compounds $[M(Cp^*)_2(terpy)]I$ (M = U, Ce).[10q] These greatest deviations were accounted for by the softer character and better π-accepting ability of the phosphorus- and nitrogen-containing ligands. The shortening of the U−S bonds with respect to the Ln−S bonds in the analogous complexes **4**–**7** is quite identical to that measured in $[M(SAr^*)_3]$ (M = U, La, Nd, Pr),[10t] $[M(Cp^*)_2(dddt)]^-$ (M = U, Ce, Nd; dddt = 5,6-dihydro-1,4-dithiine-2,3-dithiolate),[10s] and $[MI_3(1,4,7\text{-trithiacyclononane})(MeCN)_2]$ (M = U, La),[10i] the only other analogous 4f- and 5f-element compounds with a sulfur ligand to have been crystallographically characterized. The average U−C distance in **4** also exhibits a deviation of 0.03 Å with respect to the corresponding bond lengths in the lanthanide(III) counterparts, although the plot of the latter as a function of the metal ionic radii is not perfectly linear, with a r^2 factor of 0.91; this difference is similar to that observed between the U−C and Ln−C distances in other analogous trivalent cyclopentadienyl complexes.[10n,s]

In striking contrast to the $U-N_{ax}$ bond, the $U-N_{eq}$ bonds of **4** are not shortened with respect to the corresponding bonds in the lanthanide counterparts **5**–**7**, as shown by the linear plot of the average $M-N_{eq}$ distances as a function of the metal ionic radii; the r^2 factors of the regression lines, by including or not the dot corresponding to the U(III) complex, are 0.9927 and 0.9935, respectively. Thus, there is no evidence for any difference in the nature of the $M-N_{eq}$ bonds; such a situation was encountered with the M−O bonds of the $[M(OSO_2CF_3)_2(OPPh_3)_4]^+$ cations (M = U, Ce, Nd, Lu, Sc).[10k]

The distinct variations in the lengths of the axial and equatorial U−N bonds with respect to the corresponding Ln-N distances in the anions of complexes **4**–**7** reveal for the first time that anisotropy and directional effects in metal–ligand bonding can play a significant role in lanthanide(III)/actinide(III) differentiation. The structural differences in the series of $[M(Cp^*)(SBT)_3]^-$ anions could be explained by considering that the axial bonds of the pentagonal bipyramidal complexes have a more covalent character than the equatorial bonds. As a result, the $M-N_{ax}$ distances are shorter than the $M-N_{eq}$ distances, whatever the metal, the phenomenon being enhanced in the U(III) compound versus the Ln(III) analogues. The nature of the bonding in the $[M(Cp^*)(SBT)_3]^-$ anions is substantiated by a detailed DFT analysis of their electronic structure.

Molecular Geometry Optimizations. The molecular geometry optimizations of the $[M(Cp^*)(SBT)_3]^-$ complexes have been performed using the DFT/ZORA/BP86/TZP approach (see the Computational Details) starting from the coordinates given by the X-ray diffraction analysis. The calculated structural parameters are in good agreement with the crystallographic data, the bond lengths being generally slightly overestimated by 0.02–0.04 Å with a maximum deviation of 0.075 Å (Table 2). In particular, the axial M−N bonds are shorter than the equatorial ones, and the M−S bonds of the SBT ligands A and C are shorter than those of ligand B, in accordance with experiment. The shortening of the U−S bonds with respect to the Ln−S bonds is also well reproduced, with a value of 0.07 vs 0.04 Å from the crystal structures, and the deviations of the calculated $U-N_{ax}$ and $U-N_{eq}$ distances from the linear plot of the corresponding Ln−N distances are different, with values of 0.09 and 0.04 Å, respectively (vs 0.06 and ca. 0 Å),

Table 2. Comparison of Experimental and Calculated (in Square Brackets) Bond Lengths (Å)

	M–N(1A)	M–N(1B)	M–N(1C)	M–S(1A)	M–S(1B)	M–S(1C)	<M–C>
[U(Cp*)(SBT)$_3$]	2.541(3) [2.598]	2.448(4) [2.486]	2.541(3) [2.602]	2.8264(10) [2.864]	2.8736(11) [2.844]	2.8151(11) [2.854]	2.72(2) [2.732]
[U(Cp*)(SBT)$_3$]$^-$	2.662(5) [2.674]	2.562(5) [2.556]	2.643(5) [2.654]	2.9081(16) [2.922]	2.9704(17) [2.982]	2.9758(15) [2.983]	2.768(4) [2.745]
[La(Cp*)(SBT)$_3$]$^-$	2.659(7) [2.731]	2.632(7) [2.675]	2.658(7) [2.729]	2.987(2) [3.046]	3.025(2) [3.066]	2.993(2) [3.047]	2.82(2) [2.866]
[Ce(Cp*)(SBT)$_3$]$^-$	2.639(8) [2.697]	2.610(9) [2.631]	2.636(8) [2.693]	2.966(3) [3.006]	2.995(3) [3.023]	2.976(3) [3.007]	2.78(2) [2.829]
[Nd(Cp*)(SBT)$_3$]$^-$	2.614(7) [2.686]	2.578(7) [2.603]	2.611(8) [2.685]	2.926(3) [2.986]	2.961(3) [3.008]	2.941(2) [2.987]	2.777(3) [2.807]

Table 3. Mulliken Population Analysis

	metal		ligand net charge			
structure/free metallic ion/spin state	spin density (n_M)	net charge	N(1B)	N(1A,C)	S(1B)	S(1A,C)
[La(Cp*)(SBT)$_3$]$^-$/La^{3+} (4f^0)/singlet		+1.44	−0.37	−0.37	−0.40	−0.33
[Ce(Cp*)(SBT)$_3$]$^-$/Ce^{3+} (4f^1)/doublet	1.03	+1.43	−0.37	−0.37	−0.39	−0.32
[Nd(Cp*)(SBT)$_3$]$^-$/Nd^{3+} (4f^3)/quartet	3.24	+1.42	−0.37	−0.37	−0.40	−0.33
[U(Cp*)(SBT)$_3$]$^-$/U^{3+} (5f^3)/quartet	2.89	+0.98	−0.32	−0.36	−0.32	−0.26
[U(Cp*)(SBT)$_3$]/U^{4+} (5f^2)/triplet	2.20	+1.00	−0.31	−0.37	−0.24	−0.18

Table 4. Calculated Mulliken Atom−Atom α + β Overlap Populations

structure/spin state	M−N(1B)	M−N(1A,C)	M−S(1B)	M−S(1A,C)
[La(Cp*)(SBT)$_3$]$^-$/singlet	0.037	0.035–0.036	0.095	0.125–0126
[Ce(Cp*)(SBT)$_3$]$^-$/doublet	0.040	0.038–0.040	0.099	0.127–0.129
[Nd(Cp*)(SBT)$_3$]$^-$/quartet	0.042	0.038–0.041	0.110	0.137–0.139
[U(Cp*)(SBT)$_3$]$^-$/quartet	0.059	0.042–0.045	0.149	0.145–0.171
[U(Cp*)(SBT)$_3$]/triplet	0.065	0.048–0.050	0.174	0.179–0.184

confirming the specific role of the axial M−N bond in this Ln^{III}/An^{III} differentiation. Indeed, both the computed and experimental M–N$_{ax}$ distances in the anionic U(III) species [U(Cp*)(SBT)$_3$]$^-$ (2.556 and 2.562 Å) are shorter than in the Nd(III) analogue (2.603 and 2.578 Å), while all the computed M−N$_{eq}$ distances are consistent with the variation in the radii of the M^{3+} ions.[25] As expected from the respective ionic radii, the shortening of all bond lengths is observed when passing from the U(III) to the U(IV) complex.

Electronic Population Analysis. The results of the Mulliken population analysis are given in Tables 3 and 4. The metallic spin densities n_M and the metallic net charges are given in the first two columns of Table 3. Except for the U(III) complex, the value of n_M, which represents the difference between the total α and β electronic populations of the metal, is slightly higher than the number of unpaired electrons whatever the [M(Cp*)(SBT)$_3$]^q species. This means that for the latter complexes a small negative spin density is spread over the ligands. On the contrary the n_M value for the uranium(III) species is lower than 3; this suggests the occurrence of a metal-to-ligand back-donation.

The Mulliken analysis shows a significantly smaller metallic net charge for the uranium complexes than for their lanthanide counterparts. These differences can be explained by a greater ligand-to-metal donation in the former species; this fact is also evidenced by the sulfur negative net charges which are smaller in the uranium complexes than in the lanthanide ones.

The computed M−N and M−S atom-atom overlap populations are listed in Table 4. The distinct nature of the U−N bonds is clearly evidenced by the electronic structure analysis. The Mulliken analysis indicates that the spin-unrestricted overlap population of the U−N$_{ax}$ bond (0.059) is significantly larger than that of the U−N$_{eq}$ bond (0.043), whereas those of the axial and equatorial Ln−N bonds are of the same order of magnitude and do not exceed 0.042 for the Ln−N$_{ax}$ bonds. Alternatively, the net charge of the apical nitrogen atom in [U(Cp*)(SBT)$_3$]$^-$ is less negative than that of the equatorial nitrogen atoms, i.e., –0.32 vs –0.36, whereas it is strictly the same, –0.37, for all the lanthanide species. These results suggest that the unusual structural features of [U(Cp*)(SBT)$_3$]$^-$ may be attributed to the occurrence of a specific U−N$_{ax}$ bonding interaction with a significant degree of covalence.

The Mayer analysis[26] provides spin-unrestricted orbital−orbital overlap populations and atom−atom bond orders (Table 5) which have been shown to be useful tools in inorganic chemistry;[27] the given populations are the sum of the α and β spin contributions. The orbital−orbital populations between the d and f metallic orbitals (5d, 4f for the lanthanides and 6d, 5f for uranium) and the sulfur 3p and nitrogen 2p orbitals of the SBT ligands are given. It appears that the orbital−orbital populations between the nitrogen 2p orbital and the d and f metal orbitals are larger for the uranium than for the lanthanide complexes, with a contribution of the f orbitals much more important in the actinide compound. Thus, the 4f(Ln)−2p(N) and 5d(Ln)−2p(N) populations are equal to ca. 0.010 and 0.030 for N$_{ax}$ and N$_{eq}$, whereas the 5f(U)−2p(N) and 6d(U)−2p(N) populations amount, respectively, to 0.025 and 0.036 for N$_{eq}$ and to 0.046 and 0.041 for N$_{ax}$. Moreover, the bond order of the U−N$_{ax}$ bond, 0.159, is much larger than the Ln−N bonds one (maximum value of 0.096 for the neodymium derivative), whereas the difference between the U−N$_{eq}$ and Nd−N$_{eq}$ bond order is smaller (i.e., 0.103 versus 0.084), giving further evidence for a strong and specific interaction between the uranium and apical nitrogen atoms. It can also be seen that the covalent character of the metal to ligands bonds is higher in the U(IV) complex especially for the U−S bonding involving the 6d metal orbitals, and particularly that covalence is increased for the U−N$_{ax}$ bonding when passing from the U(III) to the U(IV) complex, the atom−atom bond order going from 0.159 to 0.193.

Molecular Orbital Analysis. The frontier MOs of the two isoelectronic U(III) and Nd(III) complexes in their quartet state are displayed in Figure 4. The energy gaps between different MO blocks are indicative of the occurrence of significant covalent interactions between metal orbitals and ligands. In our case, the splitting of the levels between the bonding and non bonding MOs in the uranium(III) species is higher than that in the neodymium(III) one. In the former, this energy difference between α spin MOs is equal to 2.39 eV, whereas it is equal to 0.94 eV in the neodymium counterpart. The three unpaired electrons in the two Nd(III) and U(III) complexes, occupying the SOMO, SOMO-1, and SOMO-2 numbered 110, 109, and 108, respectively, show significant differences; while they are essentially metallic in the neodymium(III) complex, those of the uranium(III)

(26) Mayer, I. *Chem. Phys. Lett.* **1983**, *97*, 270.
(27) Bridgeman, A. J.; Cavigliasso, G.; Ireland, I.; Rothery, J. *J. Chem. Soc., Dalton Trans.* **2001**, 2095.

Table 5. Mayer Orbital−Orbital Populations and Atom−Atom Bond Orders

		orbital−orbital population ligand np orbital				atom−atom bond order			
structure/spin state	metal orbital[a]	S(1A,C)	S(1B)	N_{eq}	N_{ax}	S(1A,C)	S(1B)	N_{eq}	N_{ax}
$[La(Cp^*)(SBT)_3]^-$/singlet	d	0.084	0.073	0.027	0.029	0.23	0.22	0.090	0.091
	f	0.016	0.015	0.011	0.013				
$[Ce(Cp^*)(SBT)_3]^-$/doublet	d	0.085	0.071	0.028	0.031	0.19	0.17	0.083	0.088
	f	0.015	0.015	0.011	0.012				
$[Nd(Cp^*)(SBT)_3]^-$/quartet	d	0.081	0.066	0.027	0.030	0.20	0.16	0.084	0.096
	f	0.010	0.010	0.008	0.011				
$[U(Cp^*)(SBT)_3]^-$/quartet	d	0.080	0.076	0.036	0.041	0.31	0.28	0.103	0.159
	f	0.066	0.055	0.025	0.046				
$[U(Cp^*)(SBT)_3]$/triplet	d	0.103	0.083	0.035	0.042	0.39	0.34	0.115	0.193
	f	0.078	0.064	0.029	0.055				

[a] 5d, 4f for Ln and 6d, 5f for uranium.

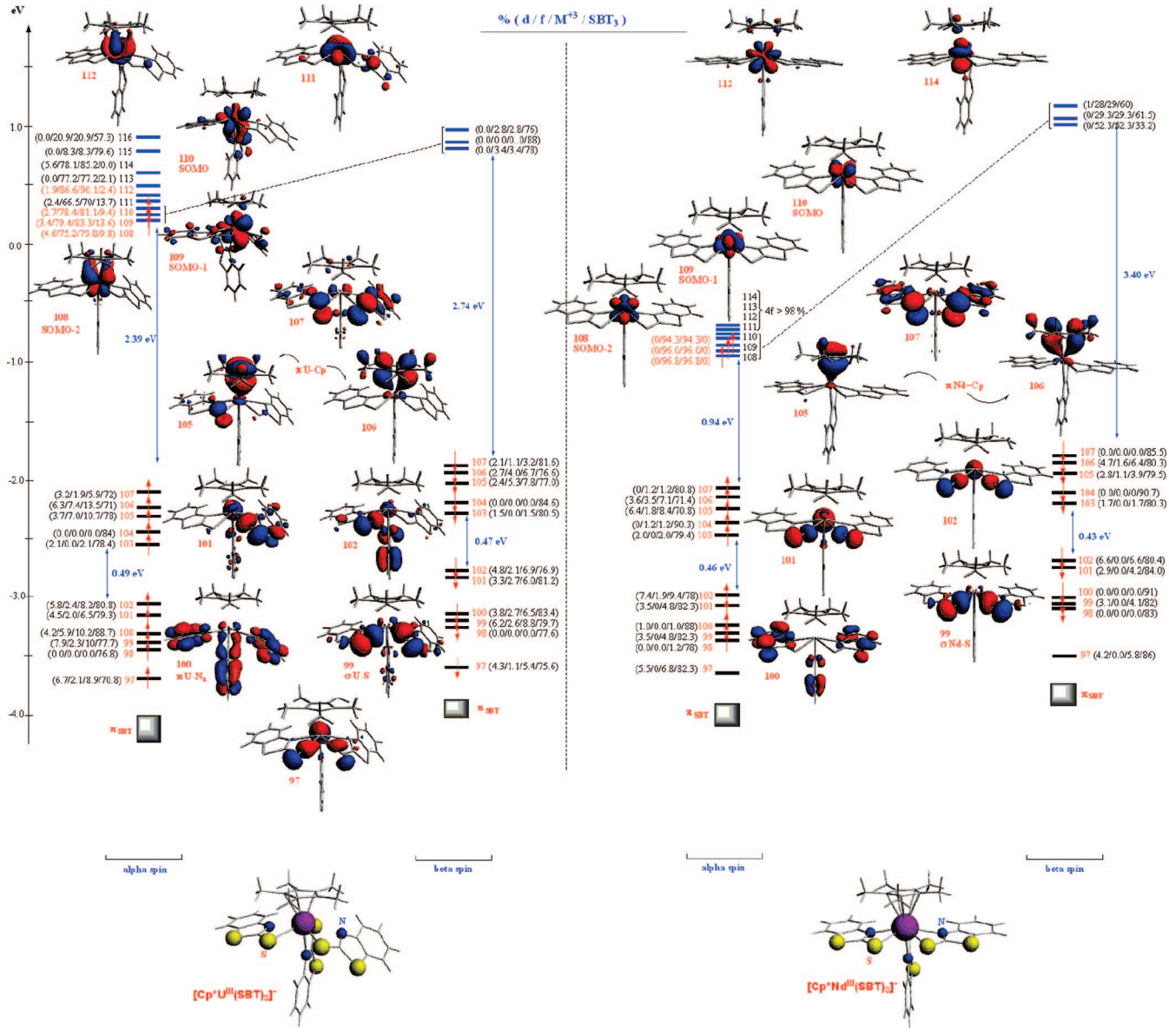

Figure 4. Comparative MO diagrams of the uranium(III) $[U(Cp^*)(SBT)_3]^-$ and neodymium(III) $[Nd(Cp^*)(SBT)_3]^-$ anionic complexes in their quartet state.

species reveal a 5f orbital−ligand mixing with a back-donation character. As a consequence the splitting of the f block (MOs 108–114) is more important for the U(III) than the Nd(III) complex. As can also be seen on figure 4, the bonding MOs (97–107) exhibit a higher contribution of the 5f actinide orbitals than the 4f lanthanide orbitals to the metal–ligands bonding, confirming the results of the population analysis.

Table 6. Total Bonding Energy (eV) Decomposition Terms for the $[M(Cp^*)(SBT_{eq})_2]^q + [SBT_{ax}]^-$ Systems

M (ion)	ΔE_{steric}	ΔE_{orb}	ΔE_{bond}
La^{3+}	−16.65	−6.46	−23.11
Ce^{3+}	−16.07	−8.82	−24.89
Nd^{3+}	−15.12	−8.31	−23.43
U^{3+}	−13.85	−12.72	−26.57
U^{4+}	−13.50	−16.28	−29.78

Total Bonding Energy Decomposition. The ADF package also supplies a decomposition of metal to ligand bonding energy into chemically useful terms.[28] The bonding energy ΔE_{bond} between two fragments is decomposed into $\Delta E_{bond} = \Delta E_{steric} + \Delta E_{orb}$ where ΔE_{steric} is the steric interaction energy between the two fragments and ΔE_{orb} is the orbital contribution to the bonding energy. The steric energy comprises the destabilizing interactions between occupied MOs and the classical electrostatic interaction between the fragments; ΔE_{orb} accounts for electron pair bonding, charge transfer, and orbital polarization.

In order to characterize energetically the specific interaction under consideration, we considered the $[M(Cp^*)(SBT_{eq})_2]^q$ species (M = La, Ce, Nd, U and $q = 0$; M = U and $q = 1$) as a molecular fragment and studied its interaction with the $[SBT_{ax}]^-$ moiety. The obtained energy decomposition is given in Table 6. Considering ΔE_{bond} we first note that the uranium species are more stabilized than the lanthanide complexes, the values for the latter being very close to each other. However it can be seen that for the lanthanide species, the steric contribution is always more stabilizing, as expected from the larger Ln−ligand vs U−ligand distances. On the contrary, ΔE_{orb} is much more important for the uranium complexes, the highest value being for the U(IV) one. This is due to the more important orbital mixing occurring between the metal and the SBT_{ax} moiety that we discussed earlier. Thus, the bonding energy decomposition analysis fully confirms the specific nature of the binding site under consideration.

Conclusion

The first SBT complexes of uranium, $[U(Cp^*)(SBT)_3]$ and $[U(Cp^*)_2(SBT)_2]$, were synthesized by treating $[U(Cp^*)(BH_4)_3]$ and $[U(Cp^*)_2Cl_2]$ with KSBT. The monocyclopentadienyl complex was reduced into the corresponding anionic uranium(III) derivative, the crystal structure of which was compared with those of the lanthanide counterparts $[Ln(Cp^*)(SBT)_3]^-$ (Ln = La, Ce, Nd). As previously observed in a number of analogous pairs of trivalent lanthanide and uranium complexes, the U−C and U−S distances are shorter than those expected from a purely ionic bonding model. However, in these pentagonal bipyramidal compounds, the $M-N_{ax}$ bonds are shorter than the $M-N_{eq}$ bonds, and the shortening of the U−N distance with respect to the Ln−N distances is observed only with the $U-N_{ax}$ bond. Consideration of the orbital interactions between ligands and metals reveals the importance of 5f uranium orbital mixing relative to the lanthanide 4f orbital one. The bond order of the $U-N_{ax}$ bond, 0.159, is much larger than the Ln−N bonds one (maximum value of 0.096 for the neodymium derivative), whereas the difference between the $U-N_{eq}$ and $Nd-N_{eq}$ bond order is smaller (i.e., 0.103 versus 0.084), giving further evidence for a strong and specific interaction between the uranium and apical nitrogen atoms. These structural features, which are confirmed by an analysis of the bonding energy, reflect the more covalent character of the axial bond which thus represents a specific covalent binding site in the differentiation of the isostructural lanthanide(III) and actinide(III) compounds.

(28) (a) Ziegler, T. *Theor. Chim. Acta* **1977**, *46*, 1. (b) de Velde, G. T.; Bickelhaupt, F. M.; van Gisbergen, S. J. A.; Guerra, C. F.; Baerends, E. J.; Snijders, J. G.; Ziegler, T. *J. Comput. Chem.* **2001**, *22*, 931.

Experimental Section

All reactions were carried out under argon with the rigorous exclusion of air and water (<5 ppm oxygen or water) using standard Schlenk vessel and vacuum line techniques or in a glovebox. Solvents were thoroughly dried by standard methods and distilled immediately before use. The ^{1}H NMR spectra were recorded on a Bruker DPX 200 instrument and referenced internally using the residual protio solvent resonances relative to tetramethylsilane (δ 0); the spectra were recorded at 23 °C when not otherwise specified. Elemental analyses were performed by Analytische Laboratorien at Lindlar (Germany). HSBT, 15-crown-5, and 18-crown-6 (Fluka) were dried under vacuum before use. $[U(Cp^*)_2Cl_2]$,[12] $[U(Cp^*)(BH_4)_3]$,[13] $[Ln(BH_4)_3(THF)_3]$ (Ln = Ce,[14a] Nd,[14b]) were synthesized as previously reported. KSBT was prepared by dropwise addition of a solution of HSBT (2.22 g, 13.3 mmol) in THF (30 mL) to a suspension of KH (0.53 g, 13.3 mmol) in THF; after stirring for 15 min at 20 °C, the yellow solution was filtered and evaporated to dryness, leaving a yellow powder of KSBT (2.48 g, 92%). ^{1}H NMR (pyridine-d_5): δ 7.59 (d, $J = 7$ Hz, 1 H), 7.45 (d, $J = 8$ Hz, 1 H), 7.15 (s, 1 H), 7.05 (s, 1 H).

Synthesis of $[U(Cp^*)_2(SBT)Cl]$ (1). A flask was charged with $[U(Cp^*)_2Cl_2]$ (94 mg, 0.16 mmol) and KSBT (33 mg, 0.16 mmol), and THF (20 mL) was condensed in it. After being stirred for 3 h at 20 °C, the orange solution was filtered and evaporated to dryness. The residue was dried under vacuum and extracted with toluene (20 mL). The solvent was evaporated off, and the brown powder of **1** was dried under vacuum. Yield: 105 mg (92%). Anal. Calcd for $C_{27}H_{34}ClNS_2U$: C, 45.66; H, 4.83; S, 9.03. Found: C, 45.92; H, 4.73; S, 8.92. ^{1}H NMR (THF-d_8): 12.34 (s, 30 H, Cp*), 0.56 (t, $J = 7$ Hz, 1 H, SBT), –1.39 (d, $J = 8$ Hz, 1 H, SBT), –1.75 (t, $J = 7$ Hz, 1 H, SBT), –22.87 (d, $J = 8$ Hz, 1 H, SBT).

Synthesis of $[U(Cp^*)_2(SBT)_2]$ (2). A flask was charged with $[U(Cp^*)_2Cl_2]$ (195 mg, 0.34 mmol) and KSBT (174 mg, 0.85 mmol), and THF (30 mL) was condensed in it. After being stirred for 12 h at 20 °C, the red solution was evaporated to dryness; the residue was dried under vacuum and extracted with toluene (30 mL). The solvent was evaporated off, and the brown powder of **2** was dried under vacuum. Yield: 269 mg (95%). Anal. Calcd for $C_{34}H_{38}N_2S_4U$: C, 48.56; H, 4.55; N, 3.33; S, 15.25. Found: C, 48.62; H, 4.66; N, 3.45; S, 15.39. ^{1}H NMR (toluene-d_8): δ 17.58 (s, 30 H, Cp*), 5.59 (t, $J = 8$ Hz, 2 H, SBT), 4.52 (t, $J = 8$ Hz, 2 H, SBT), 4.24 (d, $J = 8$ Hz, 2 H, SBT), 1.53 (d, $J = 8$ Hz, 2 H, SBT). Brown crystals of **2**·THF were deposited from a concentrated THF solution.

Synthesis of $[U(Cp^*)(SBT)_3]$ (3). A flask was charged with $[U(Cp^*)(BH_4)_3]$ (165 mg, 0.39 mmol) and KSBT (243 mg, 1.18 mmol), and THF (20 mL) was condensed in it. After being stirred for 30 min at 20 °C, the red solution was filtered, the solvent was evaporated off, and the red powder of **3** dried under vacuum. Yield: 284 mg (83%). Anal. Calcd for $C_{31}H_{27}N_3S_6U$: C, 42.70; H, 3.12; N, 4.82; S, 22.06. Found: C, 42.53; H, 3.27; N, 4.72; S, 21.97. ^{1}H NMR (THF-d_8): δ 96.48, 32.78, 30.07 and 25.76 (s, 4 × 1 H, SBT), 13.20 (s, 15 H, Cp*), –0.81, –1.24, –7.31 and –47.51 (s, 4 × 2 H, SBT). Coalescence of the signals occurred at ca. 100 °C, and the high limit spectrum could not be obtained. Red crystals were deposited from a concentrated THF solution.

Synthesis of $[Na(18\text{-crown-}6)(THF)][U(Cp^*)(SBT)_3]$. A flask was charged with $[U(Cp^*)(SBT)_3]$ (80 mg, 0.92 mmol) and 18-crown-6 (25 mg, 0.96 mmol), and THF (15 mL) was condensed in it. After addition of 2% Na(Hg) (110 mg, 1.04 mmol), the reaction mixture was stirred for 12 h at 20 °C; the color of the solution turned from orange to brown. The solution was filtered and the

Table 7. Crystal Data and Structure Refinement Details

	$[U(cp^*)_2(SBT)_2]\cdot THF$	$[U(cp^*)(SBT)_3]$	$[K(18\text{-crown-6})(THF)_2][U(cp^*)(SBT)_3]$	$[K(15\text{-crown-5})_2][La(cp^*)(SBT)_3]\cdot THF$	$[K(15\text{-crown-5})_2][Ce(cp^*)(SBT)_3]\cdot THF$	$[K(15\text{-crown-5})_2][Nd(cp^*)(SBT)_3]\cdot THF$
empirical formula	$C_{38}H_{46}N_2OS_4U$	$C_{31}H_{27}N_3S_6U$	$C_{51}H_{67}KN_3O_8S_6U$	$C_{55}H_{75}KLaN_3O_{11}S_6$	$C_{55}H_{75}CeKN_3O_{11}S_6$	$C_{55}H_{75}KN_3NdO_{11}S_6$
M_r	913.04	871.95	1319.57	1324.55	1325.76	1329.88
cryst syst	monoclinic	monoclinic	triclinic	orthorhombic	orthorhombic	orthorhombic
space group	$P2_1/c$	$P2_1/c$	$P\bar{1}$	*Pbca*	*Pbca*	*Pbca*
a/Å	23.094(2)	9.6320(6)	11.5158(5)	25.1934(11)	25.1464(19)	25.0619(13)
b/Å	10.1344(10)	8.1686(3)	12.3498(7)	23.1439(15)	23.1691(11)	23.1566(7)
c/Å	16.2740(11)	39.303(2)	21.6525(12)	21.3284(7)	21.3386(16)	21.2957(11)
α /deg	90	90	90.184(3)	90	90	90
β /deg	110.602(5)	94.286(3)	93.485(3)	90	90	90
γ /deg	90	90	114.484(3)	90	90	90
V/Å^3	3565.2(5)	3083.7(3)	2795.9(3)	12436.0(11)	12432.3(14)	12358.9(10)
Z	4	4	2	8	8	8
D_{calcd}/g cm^{-3}	1.701	1.878	1.567	1.415	1.417	1.429
μ (Mo Kα)/mm^{-1}	4.820	5.698	3.254	1.012	1.058	1.168
F(000)	1808	1688	1330	5488	5496	5512
no. of rflns collected	38959	32098	19266	214216	152354	138722
no. of indep rflns	6615	5808	9766	11603	11434	11460
no. of obsd rflns ($I > 2\sigma(I)$)	5131	4739	8260	8570	5546	6861
R_{int}	0.068	0.068	0.057	0.029	0.082	0.043
no. of params refined	425	375	649	675	699	699
R1	0.033	0.029	0.045	0.099	0.104	0.096
wR2	0.068	0.067	0.104	0.307	0.324	0.307
S	1.037	0.991	1.044	1.053	1.048	1.099
$\Delta\rho_{min}$/e Å^{-3}	−0.94	−0.80	−1.35	−1.58	−2.30	−0.94
$\Delta\rho_{max}$/e Å^{-3}	1.83	0.82	1.50	2.45	1.64	2.49

solvent evaporated off, leaving a brown powder of [Na(18-crown-6)(THF)][U(Cp*)(SBT)$_3$] which was dried under vacuum. Yield: 89 mg (79%). Anal. Calcd for $C_{47}H_{59}N_3O_7S_6NaU$: C, 45.84; H, 4.83; N, 3.41; S, 15.62. Found: C, 45.65; H, 4.84; N, 3.50; S, 15.31. ^{1}H NMR (THF-d_8, −55 °C): δ 32.22, 25.83, 18.85 and 16.06 (s, 4 × 1 H, SBT), 3.92 (s, 24 H, 18-crown-6), 2.93 (s, 2 H, SBT), −1.66 (s, 2 H, SBT), −8.76 (s, 15 H, Cp*), −9.24 (s, 2 H, SBT), −23.94 (s, 2 H, SBT). Coalescence of the signals occurred at ca. 5 °C, and the high limit spectrum could not be obtained.

Crystals of [K(18-crown-6)(THF)$_2$][U(Cp*)(SBT)$_3$] (4). An NMR tube was charged with **3** (10.0 mg, 0.011 mmol) and 18-crown-6 (3.0 mg, 0.011 mmol) in THF (0.4 mL). After addition of 2% K(Hg) (22.5 mg, 0.012 mmol), the reaction mixture was stirred for 12 h at 20 °C. Slow diffusion of pentane into the brown solution led to the formation of dark brown crystals of **4** suitable for X-ray diffraction.

Synthesis of [K(THF)$_2$La(Cp*)(SBT)$_3$]. KSBT (114 mg, 0.555 mmol) was added to a solution of [La(BH$_4$)$_3$(THF)$_3$] (74 mg, 0.185 mmol) in THF (30 mL). The reaction mixture was stirred for 2 h at 20 °C, and the pale yellow solution was filtered. After addition of KCp* (32.3 mg, 0.185 mmol), stirring for 30 min at 20 °C, and filtration, the solvent was evaporated off, leaving an off-white powder of [K(THF)$_2$La(Cp*)(SBT)$_3$] which was dried under vacuum. Yield: 126 mg (71%). Anal. Calcd for $C_{39}H_{43}N_3O_2S_6KLa$: C, 48.99; H, 4.53; N, 4.40; S, 20.12. Found: C, 48.69; H, 4.41; N, 4.51; S, 19.81. ^{1}H NMR (THF-d_8): δ 8.03 (d, J = 8 Hz, 3 H, SBT), 7.25 (d, J = 8 Hz, 3 H, SBT), 7.03 (t, J = 8 Hz, 3 H, SBT), 6.85 (t, J = 8 Hz, 3 H, SBT). Coalescence of the signals occurred at ca. −10 °C. ^{1}H NMR (THF-d_8, −85 °C): δ 8.34 (d, J = 8 Hz, 2 H, SBT), 7.79 (d, J = 8 Hz, 1 H, SBT), 7.50 (d, J = 8 Hz, 2 H, SBT), 7.32 (d, J = 8 Hz, 1 H, SBT), 7.21 (t, J = 8 Hz, 2 H, SBT), 7.05 (t, J = 8 Hz, 3 H, SBT), 6.85 (t, J = 8 Hz, 1 H, SBT).

Synthesis of [K(THF)$_2$Ce(Cp*)(SBT)$_3$]. The yellow powder of the cerium compound was prepared by following the same procedure as for the lanthanum analogue, from [Ce(BH$_4$)$_3$(THF)$_3$] (150 mg, 0.37 mmol), KSBT (230 mg, 1.12 mmol), and KCp* (67 mg, 0.38 mmol). Yield: 322 mg (90%). Anal. Calcd for $C_{39}H_{43}N_3O_2S_6KCe$: C, 48.93; H, 4.53; N, 4.39; S, 20.10. Found: C, 48.65; H, 4.55; N, 4.56; S, 19.94. ^{1}H NMR (pyridine-d_5, −10 °C): δ 24.81, 11.46, 10.87 and 10.09 (s, 4 × 1 H, SBT), 6.79, 6.08, 4.86 and −1.66 (s, 4 × 2 H, SBT), 3.97 (s, 15 H, Cp*), 3.61 (m, 8 H, THF), 1.54 (m, 8 H, THF). Coalescence of the signals occurred at ca. 10 °C and the high limit spectrum could not be obtained.

Synthesis of [K(THF)$_2$Nd(Cp*)(SBT)$_3$]. The blue powder of the neodymium compound was prepared by following the same procedure as for the lanthanum analogue, from [Nd(BH$_4$)$_3$(THF)$_3$] (59.9 mg, 0.15 mmol), KSBT (91.2 mg, 0.44 mmol), and KCp* (28 mg, 0.16 mmol). Yield: 86 mg (60%). Anal. Calcd for $C_{39}H_{43}N_3O_2S_6KNd$: C, 48.72; H, 4.51; N, 4.37; S, 20.01. Found: C, 48.52; H, 4.58; N, 4.39; S, 19.80. ^{1}H NMR (pyridine-d_5, −10 °C): δ 29.76, 14.83, 13.35 and 12.35 (s, 4 × 1 H, SBT), 9.97 (s, 15 H, Cp*), 6.13, 5.11, 3.20 and −7.82 (s, 4 × 2 H, SBT), 3.61 (m, 8 H, THF), 1.54 (m, 8 H, THF). Coalescence of the signals occurred at ca. 30 °C, and the high limit spectrum could not be obtained.

Crystals of [K(15-crown-5)$_2$][Ln(Cp*)(SBT)$_3$]·THF (5–7). An NMR tube was charged with [K(THF)$_2$Ln(Cp*)(SBT)$_3$] (10.0 mg, 0.010 mmol) and 15-crown-5 (5.0 mg, 0.023 mmol). Slow diffusion of pentane into the solution led to the formation of colorless (Ln = La), yellow (Ln = Ce) or blue (Ln = Nd) crystals of [K(15-crown-5)$_2$][Ln(Cp*)(SBT)$_3$]•THF suitable for X-ray diffraction.

Crystallographic Data Collection and Structure Determination. The data were collected at 100(2) K on a Nonius Kappa-CCD area detector diffractometer[29] with graphite-monochromated Mo Kα radiation (λ = 0.71073 Å). The crystals were introduced into glass capillaries with a protective "Paratone-N" oil (Hampton Research) coating. The unit cell parameters were determined from 10 frames and then refined on all data. The data (φ and ω scans with 2° steps) were processed with HKL2000.[30] The structures were solved by direct methods or by Patterson map interpretation with SHELXS97 and subsequent Fourier-difference synthesis and refined by full-matrix least-squares on F^2 with SHELXL97.[31] Absorption effects were corrected empirically with DELABS[32] or SCALEPACK.[30] All non-hydrogen atoms were refined with anisotropic displacement parameters. The hydrogen atoms were intro-

(29) Kappa-CCD Software; Nonius BV: Delft, 1998.
(30) Otwinowski, Z.; Minor, W. *Methods Enzymol.* **1997**, *276*, 307.
(31) Sheldrick, G. M. SHELXS97 and SHELXL97; University of Göttingen, 1997.
(32) Spek, A. L. PLATON; University of Utrecht, 2000.

duced at calculated positions and were treated as riding atoms with an isotropic displacement parameter equal to 1.2 (CH, CH_2) or 1.5 (CH_3) times that of the parent atom. Special details are as follows:

[K(18-crown-6)(THF)$_2$][U(Cp*)(SBT)$_3$]. One carbon atom of the THF molecule bound to K(2) is disordered over two positions which have been refined with occupancy parameters constrained to sum to unity and restraints on bond lengths, angles and displacement parameters.

[K(15-crown-5)$_2$][M(Cp*)(SBT)$_3$]·THF, M = La, Ce, Nd. The two crown ethers and the solvent THF molecules are extremely badly resolved, seemingly due to untractable disorder, and the use of many restraints on bond lengths, angles, and displacement parameters was necessary (for M = La, four atoms were refined isotropically). However, as shown by the high *R* factors and residual electron density (located near the crown ethers), as well as by several short H···H contacts, the description of these parts is very far from perfect. Fortunately, the most important part of the structure, which is the rare earth anionic complex, does not suffer from such disorder and can be confidently considered as properly characterized.

Crystal data and structure refinement details are given in Table 7. The molecular plots were drawn with SHELXTL.[33]

Computational Details. The calculations were performed using the Amsterdam Density Functional program (ADF2006.01 release).[34] We considered for all complexes the highest spin state as the ground-state in the spin unrestricted calculations, i.e., a quartet state for the anionic neodymium(III) and uranium(III) complexes, a triplet state for the neutral uranium(IV) species, a doublet for the anionic cerium(III) complex. The lanthanum(III) complex is a closed-shell system. Relativistic effects were considered through the zeroth-order regular approximation (ZORA).[34d] Triple-ζ Slater-type orbitals augmented with one set of polarization functions, i.e., the ADF ZORA/TZP basis sets, were used for the description of the valence part of all atoms; we kept their core frozen up to 4d/5d for lanthanides/actinides and up to 2p for sulfur and 1s for carbon and nitrogen atoms during molecular calculations. The core density was obtained from four-component Dirac–Slater calculations. Valence electrons spin–orbit effects were not taken into account. The Vosko−Wilk−Nusair functional[35] for the local density approximation (LDA) and the nonlocal corrections for exchange and correlation of Becke[36a] and Perdew,[36b] respectively, have been used.

Supporting Information Available: Tables of crystallographic data (CIF). This material is available free of charge via the Internet at http://pubs.acs.org.

OM7007315

(33) Sheldrick, G. M. SHELXTL, Version 5.1; Bruker AXS Inc.: Madison, WI, 1999.

(34) (a) van Lenthe, E.; Baerends, E. J.; Snijders, J. G. *J. Chem. Phys.* **1994**, *101*, 9783. (b) van Lenthe, E.; Snijders, J. G.; Baerends, E. J. *J. Chem. Phys.* **1996**, *105*, 6505. (c) Fonseca, G. C.; Snijders, J. G.; te Velde, G.; Baerends, E. J. *Theor. Chem. Acc.* **1998**, 391. (d) van Lenthe, E.; Ehlers, A.; Baerends, E. J. *J. Chem. Phys.* **1999**, *110*, 8943. (e) te Velde, G.; Bickelhaupt, F. M.; van Gisbergen, S. A. J.; Fonseca, G. C.; Baerends, E. J.; Snijders, J. G.; Ziegler, T. *J. Comput. Chem.* **2001**, 931. (f) ADF2006.01, SCM; Theoretical Chemistry, Vrije University: Amsterdam, The Netherlands; http://www.scm.com.

(35) Vosko, S. D.; Wilk, L.; Nusair, M. *Can. J. Chem.* **1990**, *58*, 1200.

(36) (a) Becke, A. D. *Phys. Rev. A* **1988**, *38*, 3098. (b) Perdew, J. P. *Phys. Rev. B* **1986**, *34*, 7406.